Modelling of the temporal and spatial evolutions of weakly nonlinear random directional waves with the modified nonlinear Schrödinger equations

Peregrine breathers as design waves for wave-structure interaction

Marco Klein[a,*], Günther F. Clauss[a], Suresh Rajendran[b], Carlos Guedes Soares[b], Miguel Onorato[c]

[a] *Ocean Engineering Division, Technische Universität Berlin, Germany*
[b] *Centre for Marine Technology and Ocean Engineering (CENTEC), Instituto Superior Técnico, Universidade de Lisboa, Portugal*
[c] *Dipartimento di Fisica, Università di Torino, Italy*

A B S T R A C T

This paper introduces the Peregrine breather solution of the nonlinear Schrödinger-type equation as an innovative design wave. The major benefits are the potential to generate abnormal waves of certain frequency up to physically possible wave heights, the symmetrical abnormal wave shape and the availability of an analytical solution. The characteristics of Peregrine breathers as well as their impact on marine structures were investigated. To evaluate the applicability of the Peregrine breather solution as design wave, wave-structure investigations with a LNG carrier were performed in a set of Peregrine breathers at certain frequencies. The investigations comprised model tests as well as numerical simulations. For the purpose of comparison, a real-world abnormal wave reproduction was additionally investigated allowing the evaluation of breather-type abnormal waves regarding the applicability as design wave. Therefore, the famous 'New Year Wave', an abnormal wave recorded in the North Sea at the Draupner jacket platform on January 1st, 1995, was selected.

1. Introduction

The existence of abnormal, freak or rogue waves is an incontrovertible fact due to many reports on observations and accidents (Faulkner and Buckley, 1997). There are reports from cruise vessels encountering freak waves, some escaped with no more than a fright whereas others suffered disastrous consequences (e.g. Schulz (2001), Lemire (2005), Bertotti and Cavaleri (2008)). In contrast to cruise ships, where the impact of steep waves at the bow will cause (dangerous) local damage at the superstructure with potentially serious consequences, cargo vessels are more affected by wave-induced global loads which may cause structural failure. Ship losses such as the sinking of the single-hull tankers Erika (1999) and Prestige (2002) as well as the double-hull tanker Ievoli Sun (2000) confirm the need for systematic investigations. A general overview on real sea abnormal wave records and reported accidents can be found in Kharif et al. (2009).

A precise knowledge of loads and motions in extreme wave sequences is indispensable for the design of ships and offshore structures to reduce the risk of serious incidents and disaster. The formation process and the frequency of occurrence of abnormal waves as well as the consequences of their impact on ships and offshore structures are still under intensive investigations. The research comprises investigation on different types of offshore structures with tubular members by Gorf et al. (2000), Suyuthi and Haver (2009), Clauss et al. (2010a, 2010b) and others in terms of local impact and by Karunakaran et al. (1997) in terms of global response. Floating structures of FPSO type have also been studied for example by Guedes Soares et al. (2006) and Fonseca et al. (2007, 2010), focusing on aspects of local impact on the bow area. Investigations by Stansberg and Karlsen (2001) revealed that the encountering wave profile in terms of wave steepness as well as the ship motions are important parameters for local loads: "relative short and steep waves are more critical than longer waves, due to the phase lag of the pitch motion", in particular in combination with large pitch amplitudes. Guedes Soares et al. (2007) has observed experimentally that the occurrence of large wave slamming loads depend on the local steepness of the waves. Besides the local impact of abnormal waves, the effect on global loads of different ship types have been intensively studied (e.g. Pastoor et al., 2003; Clauss et al., 2004; Guedes Soares et al., 2008). Watanabe et al. (1989), Rajendran et al. (2011) and Clauss et al. (2010a, 2010b, 2011a, 2011b) showed that the geometry of the bow flare in combination with the wave steepness as well as encountering wave length influences the global loads significantly, in particular the sagging loads.

Tailored wave sequences are indispensable for the evaluation of a design, be it wave events identified by numerical investigation such as design wave concepts or wave events of a more general nature such as abnormal waves embedded in irregular sea states or real-world reproductions. Abnormal wave events are of particular interest as they are outstanding situations relevant for all ships and offshore structures. The numerical and experimental modelling of such wave conditions to

be investigated in the design process is a challenging problem. Different alternatives are available to evaluate offshore structures in high, steep waves - transient wave packages (Clauss and Kühnlein, 1996), regular waves as well as irregular sea states with random phases. More sophisticated methods focus on tailored critical wave sequences such as from design wave concepts (e.g. Torhaug et al., 1998; Tromans et al., 1991; Friis-Hansen and Nielsen, 1995; Adegeest et al., 2000; Dietz, 2004), extensive numerical simulations or real-world abnormal wave reproductions (e.g. Schmittner, 2005; Fonseca et al., 2006, 2008; Clauss et al., 2006; Klein, 2015). In particular, wave/structure interaction investigations with real-world abnormal wave reproductions are indispensable for a complete understanding as they represent abnormal wave events happened on sea at which floating structures have to survive. They exclude any doubt regarding discussions on possible unrealistic, artificial wave sequences. However, such complex structures of wave sequences require sophisticated reproduction procedures as presented by Schmittner (2005), Clauss et al. (2006, 2013) as well as Schmittner and Hennig (2012) and do not represent the day-to-day business of test facilities.

Thus, a straightforward method for fast generation of realistic abnormal waves with varying characteristics is required enabling systematic investigations of abnormal wave-structure interaction. Breather solutions, which are exact solutions of the nonlinear Schrödinger-type (NLS) equation, are predestined as they are considered as prototypes for abnormal waves (Dysthe and Trulsen, 1999; Osborne et al., 2000). Henderson et al. (1999) showed that these waves feature many similarities to real-world abnormal waves and Zhang et al. (2014, 2015) showed that predictions of the NLS equation reproduce well also the mechanically generated waves on laboratory conditions. They serve as suitable analytic models simulating steep wave events (Dysthe et al., 1999) and are promising candidates for extreme wave modelling (Huijsmans et al., 2005; Andonowati et al., 2006). Altogether, three (first order) solutions are known, namely Kusnetzov-Ma breather (Kuznetsov, 1977; Ma, 1979), Akhmediev breather (Akhmediev et al., 1985, 1987; Akhmediev and Korneev, 1986) and Peregrine breather (Peregrine, 1983), which have been successfully utilized in wave tanks experiments by Chabchoub et al. (2010, 2011) and Clauss et al. (2011a, 2011b). The general applicability of breather solutions to abnormal wave-structure investigations has also already been shown by Clauss et al. (2012), Onorato et al. (2013) and Klein (2015).

The Peregrine breather is particularly in focus as this solution is localized in time and space resulting in a wave that “appears from nowhere and disappears without trace” (Akhmediev et al., 2009a, 2009b). Chabchoub et al. (2010) showed the “Experimental Evidence for Breather Type Dynamics in Freak Waves” by adjusting the Peregrine breather characteristics to real-world abnormal waves such as the New Year Wave (NYW) as well as the Yura wave (Mori et al., 2000). A detailed study on Peregrine breather characteristics in terms of breaking threshold, lifetimes and travel distance of the abnormal wave has been presented by Chabchoub et al. (2012). It has been shown that the initial wave steepness is one of the decisive parameters for wave tank experiments to adjust the maximum wave height/steepness up to breaking waves and that the abnormal wave would travel few minutes and kilometres at the ocean. In addition, this study revealed that breather solutions serve as analytical model for defining the boundary condition at the wave board but the physical waves show an increasing difference to the predicted theoretical model (exact solution as well as numerical simulations based on NLS equation) with increasing finite initial wave steepness (see also Shemer and Alperovich (2013)). In this context, Perić et al. (2015) investigated the dynamics of breaking breather waves comparing experiments with numerical simulations. They have shown that numerical simulations based on Navier-Stokes equations show an excellent agreement compared to the measured surface elevation. The dynamics during evolution as well as breaking of the abnormal wave can be investigated detailed by numerical field methods. Recently, so-called super-rogue waves have also come into focus as prototype for freak wave evolution. Super-rogue waves represent a hierarchy of higher-order rational breather solutions (Akhmediev et al., 1987, 2009a, 2009b; Dubard et al., 2010; Gaillard, 2012). Higher-order rational breather solutions are characterized by superposition of a group of rogue waves. The first order solution is the Peregrine solution. The amplitude amplification factor (AAF), which is 3 for the first order solution, depends on the order N and can reach impressive values. For order $N = 5$ with $AAF = 2{\cdot}N + 1$ results in an eleven times higher abnormal wave compared to the background amplitude. Chabchoub et al. (2012) investigated higher-order breather solutions experimentally, presenting the evolution of a second-order rational breather solution. Again, the agreement between theory and experiments is excellent for small steepness and decreases with increasing initial steepness of the solution. Based on this study, Slunyaev et al. (2013) investigated the evolution of super-rogue waves more systematically by means of numerical simulations. The focus of the study lies on variation of the order of the higher-order rational breather solution $1 \leq N \geq 5$ investigating the influence of the focussing distance on the evolution, in particular regarding the AAF. The analytical solution based on NLS equation serves as initial approximation for subsequent numerical simulations using modified NLS equation (MNLS, Dysthe, 1979) and fully nonlinear Euler equations. They showed that in contrast to the first order solution the higher-order solutions show a more distinctive deviation between the analytical solution based on NLS equation and MNLS as well as fully nonlinear simulations. Altogether, the research results on breather solutions “supports the hypothesis that the Benjamin-Feir instability correlated to breathing is a possible explanation for a sudden formation of rogue waves” (Chabchoub et al., 2010) in the real ocean. However, the evolution of breather solutions on an irregular background such as under oceanic conditions is not answered up to now. Consequentially, breather-type abnormal waves are promising candidates as design abnormal waves. The existence of an analytical solution offers a fast and simple generation of the wave maker control signal. In addition, the small frequency bandwidth offers the tailored investigation of critical wave lengths in terms of structure response as well as the wave group steepness is variable up to very steep waves. Moreover, breaking breather waves represents the maximum possible wave height at a certain wave length to be suffered by a marine structure. The potential of breather solutions as design abnormal waves for abnormal wave-structure investigations is presented in this paper by means of experimental and numerical investigations. Therefore, the Peregrine breather is chosen as an example representing the limiting case of the time-periodic Kusnetzov-Ma breather solution and the space-periodic Akhmediev breather solution. However, the results presented are directly transferable to the other two solutions (Klein, 2015). This study comprises:

- Investigation of abnormal wave characteristics in terms of wave kinematics and dynamics.
- Investigation of the potential of breather solutions for the generation of tailored extreme wave sequences. The Peregrine breather is applied for the generation of a tailored irregular sea state with embedded abnormal wave.
- Abnormal wave-structure investigations with a LNG carrier (LNGC) addressing the vertical wave bending moment amidships as well as the vertical ship motion.

For the evaluation of the applicability of breather solutions as design abnormal waves, a real-world abnormal wave reproduction, namely the New Year Wave, is additionally investigated for the purpose of comparison. The objective is to draw conclusions on the differences or similarities between the real-world NYW and the somehow artificial breather-type abnormal waves allowing conclusions regarding the applicability as well as relevance of breather solutions as design

abnormal waves.

2. Theoretical background

2.1. Breather-type abnormal waves

Assuming that the Newtonian fluid is incompressible, inviscid and irrotational, the NLS equation can be deduced from the potential water wave equations under the hypothesis of small amplitudes and quasi-monochromatic waves. The NLS equation is suitable for describing the evolution in time of a space series. For wave tank applications, time series at specific locations in space are required, e.g. at the wave board to drive the wave maker. The TNLS, where T stands for time, can be derived by an iterative procedure exchanging the derivatives in space with derivatives in time and vice versa (see e.g. Mei (1989)), resulting in

$$\frac{\partial \mathbf{A}}{\partial \mathbf{x}} + \frac{1}{\mathbf{C_g}}\frac{\partial \mathbf{A}}{\partial \mathbf{t}} + \mathbf{i}\alpha'\frac{\partial^2 \mathbf{A}}{\partial \mathbf{t}^2} + \mathbf{i}\beta'|\mathbf{A}|^2\mathbf{A} = 0 \tag{1}$$

with $\alpha' = \frac{1}{8}\frac{\omega_c}{k_c^2}\frac{\alpha}{C_g^3}$ and $\beta' = \frac{1}{2}\omega_c k_c^2 \frac{\beta}{C_g}$. The coefficients α and β are depending on the carrier wave number k_c, the corresponding angular frequency ω_c and the water depth d (Hashimoto and Ono, 1972). A remarkable feature of the coefficients α and β is that their ratio $\sqrt{\beta/\alpha}$ indicates the influence of the water depth on the modulational instability. It converges to one for $k_c d \to \infty$, decreases for decreasing water depth and becomes negative for $k_c d < 1.36$. Thereby, the ratio $k_c d = 1.36$ marks a physically important property – for $k_c d > 1.36$ the TNLS equation has focusing properties, i.e. energy can be focused through modulational instability, which is impossible for $k_c d < 1.36$

The nonlinear evolution of the modulational instability can be described by exact solutions of the NLS equation, known as breather solutions. Breather solutions are characterized by slightly perturbed quasi-monochromatic waves in time or space. The perturbation of the breather envelope increases during evolution due to modulational instability resulting in large amplification of the initial amplitude. The breather solutions have the following general form

$$A(x,\ t) = A_0(x)[G(x,\ t)\exp(i\phi(x)) - 1] \tag{2}$$

where G, ϕ are real functions to be determined and $A_0 = a_0\exp(-i\beta' a_0^2 x)$. A detailed discussion on the derivation of the three different solutions can be found in Groesen et al. (2006) and in Karjanto and Groesen (2007). At the end, the three known exact solutions of the NLS are obtained, namely the Kusnetzov-Ma breather, the Akhmediev breather and the Peregrine breather.

For this study, the Peregrine solution, (Peregrine, 1983), also known as rational solution, is investigated exclusively representing the limiting case of the time-periodic Kusnetzov-Ma breather and the space-periodic Akhmediev breather. It has the peculiarity of being not periodic in time and in space: it is a wave that "appears from nowhere and disappears without trace", (Akhmediev et al., 2009a). However, the results obtained are directly transferable to the other two solutions (Klein, 2015). Its analytical form is according to Karjanto and Groesen (2007)

$$A(x,\ t) = A_0(x)\left(\frac{4\alpha'(1 - i2\beta' a_o^2 x)}{\alpha' + \alpha'(2\beta' a_0^2 x)^2 + 2\beta' a_0^2 t^2} - 1\right) \tag{3}$$

The relation of the complex envelope $A(x,\ t)$ to the leading order of the surface elevation is

$$\zeta(x,\ t) = \frac{1}{2}(A(x,\ t)\bullet\exp(i(kx - \omega t)) + c.\ c.) \tag{4}$$

where c.c. stands for complex conjugate. For the determination of the Peregrine solution, only the plane-wave amplitude a_0 as well as carrier frequency ω_c has to be predefined. Fig. 1 presents the envelope of the Peregrine breather in time and space. The AAF due to modulational instability is always equal to three, i.e. the perturbed wave will grow to an abnormal wave reaching three times the amplitude of the selected background plane-wave. Selecting the surface elevation in time domain for a desired location in space gives the boundary condition (e.g. wave sequence at the wave board) for subsequent experimental or numerical investigations. In our case, the distance between wave board and investigated LNGC is 45 m, whereby the envelope of the $A - t$ – profile at $x = -45$ m is determined enabling to calculate the surface elevation at the wave maker and the wave maker control signal immediately. This is the major benefit of the breather solutions as only the amplitude, wave length as well as position in space domain has to be defined to generate a certain abnormal wave at once.

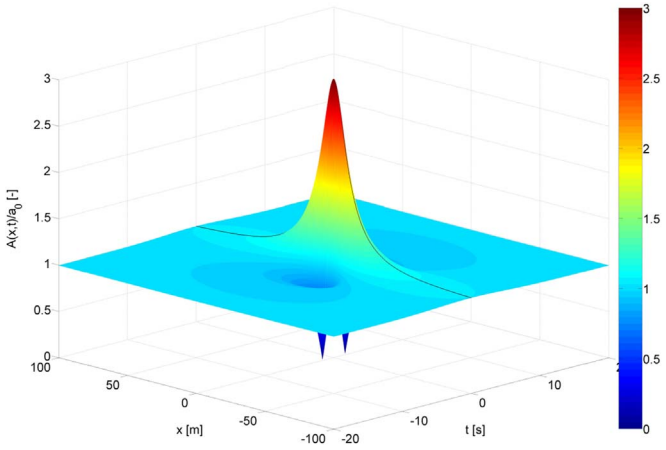

Fig. 1. Envelope of the Peregrine breather in time and space.

For the reproduction of Peregrine breather abnormal waves in the wave tank, the above presented solution has been implemented in the wave generation software in such a way that simply the carrier wave length, the initial steepness at the wave board as well as the target location of the high, steep single wave has to be defined to calculate the surface elevation at the wave board. Afterwards, the surface elevation at the wave board has been divided by the response amplitude operator (RAO) of the wave maker in frequency domain to obtain the control signal. The agreement between theoretical location of abnormal wave occurrence (input) and the registrations/observations in the tank showed satisfying agreement, i.e. the actual abnormal wave event was nearby the given value. But due to the fact that wave/structure investigations implies the definition of target waves in time domain at precise target locations, the investigated Peregrine breather presented in this paper resulting from an adjustment of the first control signal to obtain the abnormal wave as exact as possible at the target location. However, the generation process of this kind of abnormal waves is very efficient compared to established procedures for generating tailored (abnormal) wave sequences.

2.2. Numerical method for calculation of the ship response

2.2.1. Equation of motion

The ship responses are calculated using a body nonlinear time domain method based on strip theory. The numerical method is based on the formulation proposed by Rajendran et al. (2013, 2014, 2015a and 2015b). The method takes account of the surge mode in the equation of motion following a semi-empirical method for calculation of the surge hydrodynamic coefficients and exciting forces, (Rajendran et al., 2015b). Previous studies on the effect of the surge on the vertical responses showed that the axial forces due to surge influences the vertical bending moment calculated at the deck. However, its effect on the vertical motions and loads about the transverse axis at the neutral axis was negligible.

Rajendran et al. (2015a) presented a body nonlinear method to calculate the ship responses in extreme seas. The method has been developed keeping in mind that the technique should be fast, robust and accurate enough for the calculation of the short term probability distribution of the nonlinear loads in order to apply for practical engineering scenario. The Froude-Krylov and hydrostatic forces are calculated for the exact wetted surface area under the incident wave. The incident wave pressure above the mean water line is assumed to be hydrostatic. The radiation forces are expressed in terms of infinite frequency added mass, memory function and hydrodynamic restoring coefficients. The memory functions, which represent the memory effect due to the free surface, is calculated from the frequency domain coefficients based on the analogy between the Fourier transform of the time domain radiation forces and the frequency domain radiation forces.

The time domain radiation forces are calculated by:

$$F_k^R(t) = A_{kj}^{\infty}\ddot{\xi}_j(t) + \int_{-\infty}^{t} K_{kj}^m(t-\tau)\dot{\xi}_j(\tau)d\tau + C_{kj}^m\xi_j(t) \quad k,\ j=1,\ 3,\ 5 \tag{5}$$

The memory functions, K_{kj}^m, and radiation restoration coefficients, C_{kj}^m, are calculated using the following equations:

$$K_{kj}^m(t) = \frac{2}{\pi}\int_0^{\infty}(B_{kj}(\omega)\cos\omega t)d\omega \tag{6}$$

$$C_{kj}^m = \omega^2[A_{kj}^{\infty} - A_{kj}(\omega)] - \omega\int_0^{\infty}K_{kj}^m(\tau)\sin(\omega t)d\tau \quad k,\ j=1,\ 3,\ 5 \tag{7}$$

where $A_{kj}(\omega)$ and $B_{kj}(\omega)$ represent frequency dependent global added masses and damping coefficients.

In order to achieve a fully body nonlinear solution, the radiation forces are calculated for the instantaneous wetted surface area. A practical engineering technique is followed for the calculation of the body nonlinear radiation forces. In the pre-processing stage, the frequency domain hydrodynamic coefficients are calculated for a range of draft and stored in the data base. During the time domain simulation, the hydrodynamic coefficients corresponding to the exact draft under the incident wave are calculated by means of interpolation of the pre-calculated hydrodynamic coefficients. These updated coefficients are used in Eqs. (5)–(7) for the calculation of the memory functions and the hydrodynamic restoring coefficients. Since the main objective of the study is to calculate the design bending moment which occurs in head sea condition, the method focuses on the head sea condition. The diffraction forces, which can be expressed in terms of the hydrodynamic coefficients for the head sea condition, are also body nonlinear. The green water force is calculated based on momentum method Buchner (1995).

For surge, heave and pitch, the equation of motion could be written as

$$(M + A_{11}^{\infty})\ddot{\xi}_1(t) + \int_{-\infty}^{t}K_{11}(t-\tau)\dot{\xi}_1(\tau)d\tau + C_{11}\xi_1(t) + (MZ_{cg} + A_{15})\ddot{\xi}_5 + \int_{-\infty}^{t}K_{15}(t-\tau)\dot{\xi}_5(\tau)d\tau + C_{15}\xi_5(t) = F_1^E(t) \tag{8}$$

$$(M + A_{33}^{\infty})\ddot{\xi}_3(t) + \int_{-\infty}^{t}K_{33}(t-\tau)\dot{\xi}_3(\tau)d\tau + C_{33}\xi_3(t) + A_{35}\ddot{\xi}_5 + \int_{-\infty}^{t}K_{35}(t-\tau)\dot{\xi}_5(\tau)d\tau + C_{35}\xi_5(t) + F_3^H - Mg = F_3^E(t) + F_5^{gw}(t) \tag{9}$$

$$(I_{55} + A_{55}^{\infty})\ddot{\xi}_5(t) + \int_{-\infty}^{t}K_{55}(t-\tau)\dot{\xi}_5(\tau)d\tau + C_{55}\xi_5(t) + A_{53}^{\infty}\ddot{\xi}_3 + \int_{-\infty}^{t}K_{53}(t-\tau)\dot{\xi}_3(\tau)d\tau + C_{53}\xi_3(t) + (MZ_{cg} + A_{51}^{\infty})\ddot{\xi}_1 + \int_{-\infty}^{t}K_{51}(t-\tau)\dot{\xi}_1(\tau)d\tau + C_{51}\xi_1(t) + F_5^H(t) = F_5^E(t) + F_5^{gw}(t) \tag{10}$$

where ξ_1, ξ_3 and ξ_5 represent respectively surge, heave and pitch motions and dots over the symbols represent differentiation with respect to time. M is the ship mass, g is acceleration of gravity, Z_{cg} is the vertical distance between the centre of gravity of the ship and the frame of reference and I_{55} represent the ship inertia about the y-axis. The hydrostatic force and moment, F_3^H and F_5^H, are calculated at each time step by integration of the hydrostatic pressure over the wetted hull under the undisturbed wave profile. The exciting forces due to the incident waves, F_1^E, F_3^E and F_5^E, are decomposed into a diffraction part, F_1^D, F_3^D and F_5^D, and the well-known Froude-Krylov part, F_1^K, F_3^K and F_5^K. A_{jk}^{∞} (j, k=1, 3, 5) are the infinite frequency added masses, K_{jk} represent the memory functions and C_{kj}^m is the radiation restoration coefficients. F_3^{gw} and F_5^{gw} are green water force and moment.

The wave induced structural dynamic loads at a ship section are obtained from the difference between the inertia force and the sum of the hydrodynamic force acting on the part of the hull forward of the section. The method to calculate the components of the forces are consistent with the calculations for the ship motions. Here, the forces are calculated only up to the particular section of interest instead of the entire ship hull. The longitudinal shear force, vertical shear force and vertical bending moments are calculated for the sections of interest. For the bending moments, positive and negative moments denote the hogging and sagging moments, respectively.

2.2.2. Irregular waves

The experimental incident waves serve as input for the numerical simulation. The experimental wave elevation is assumed to be stationary and composed of infinite number of harmonic components. The harmonic components are extracted through Fourier transformation. In irregular long crested seas, the wave elevation can be written as

$$\zeta(t) = \sum_{n=1}^{\infty}(\zeta_a)_n\cos[(\omega_e)_n t + k_n x\cos\beta + \varepsilon_n] \tag{11}$$

where ζ_a, ω_e, ε and k are the wave amplitude, encounter frequency, phase angle and the wave number of the nth harmonic component. β and x are the heading angle of the ship and the distance from the LCG of the ship.

3. Experimental program

This study comprises experimental and numerical investigations at scale 1:70. The model scale, in combination with the seakeeping basin water depth, simulates the actual water depth at the Draupner jacket platform. At this platform, the famous NYW (Haver and Anderson, 2000) has been measured which is reproduced in the seakeeping basin as reference abnormal wave. The experimental program comprised investigations of the characteristics of breather-type abnormal waves in terms of dynamic pressure and particle velocity, their potential for tailored abnormal wave generation as well as their impact on a LNGC. The results obtained were compared to experiments with the NYW.

3.1. Test facilities

The experiments (except the experiment on tailored Peregrine breather embedded in an irregular sea state) were conducted in the seakeeping basin of the Ocean Engineering Division of Technical

University Berlin. The basin is 110 m long, with a measuring range of 90 m. The width is 8 m and the water depth is 1 m. On one side a fully computer controlled electrically driven piston type wave generator is installed. The control software features the generation of transient wave packages, deterministic irregular sea states with predefined characteristics as well as tailored critical wave sequences (Clauss and Kühnlein, 1996; Clauss and Schmittner, 2005). This technique has been established to reproduce a large variety of wave sequences such as single abnormal waves as well as groups of abnormal waves embedded in irregular sea states to investigate the response of floating structures to an extreme, but realistic, wave environment.

The experiment on the tailored Peregrine breather embedded in an irregular sea state was performed in the seakeeping basin of Canal de Experiencias Hidrodinámicas de El Pardo (CEHIPAR). This seakeeping basin is 150 m long, 30 m wide and the water depth is 5 m. The flap-type wave maker is located on one of the smaller sides, feature the same wide (30 m) and consist of 60 individual flaps, which enables also the generation of short-crested sea states. On the opposite side, a wave damping slope is installed. The wave generator is fully computer controlled and the installed software enables the generation of regular and irregular waves.

3.2. Wave characteristics

The dynamic pressure as well as the particle velocities of the NYW as well as one Peregrine breather, featuring similar wave crest characteristic, were systematically measured at different vertical positions up to the still water level and for some cases also above, up to the wave crest at target position, i.e. at position of maximum wave height and wave breaking, respectively. The pressure measurements were conducted with a pressure transducer (Bell & Howell, type BHL 4104-00-05110). Simultaneously, the particle velocities were measured by an ultrasonic flow meter featuring the measurement of the particles' velocity in three orthogonal planes (Denshi Kogyo Co. LTD, type DS-102S). Both sensors were mounted on a vertical semi-beam which was adjustable in height for the investigation of different water depths. The sensors were mounted, therefore, in such a way that the vertical measuring plane is identical and the measuring points are far enough from each other for unaffected operation. However, the geometry and measurement principle of the utilized sensors limit the operational range of the investigations. The ultrasonic flow meter cannot be used above still water level due to the measurement principle. In addition, only a short emerging in wave troughs can be compensated. The pressure sensor on the other side can be utilized above the still water level, but needs a minimum impact time interval of the wave crest to produce reasonable and trustworthy data. Both sensors cannot be utilized near the bottom of the seakeeping basin due to the geometry of the sensors, with the pressure sensor being far less applicable in this respect.

3.3. Wave-structure interaction

The abnormal wave-structure investigations were conducted with a LNGC at zero speed in head waves addressing the vertical wave bending moment amidships as well as vertical ship motions. Fig. 2 presents the equipped model of the LNGC. The main dimensions and load conditions are given in Table 1. The LNGC has been made of fiberglass reinforced plastic (GRP) subdivided into two segments at $L_{pp}/2$, being connected with three force transducers. Two of them were installed on the deck level, and one underneath the bottom of the model. The force transducers register the longitudinal forces during the model tests. Based on the measured forces and the given geometrical arrangement of the three force transducers, the resulting vertical wave bending moment and the longitudinal forces were obtained. In addition, the LNGC model was equipped with pressure transducers at bow and stern. Furthermore, two wave gauges were installed on deck at the forecastle (see blue circles in Fig. 2) to detect green water impact on deck. The ship motions were recorded by an optical tracking system. This study concentrates exclusively on the vertical bending moment and vertical motions for the evaluation of the application of breather solutions for systematic wave/structure interaction investigations.

Fig. 2. Equipped model of the LNGC. (For interpretation of the references to color in this figure, the reader is referred to the web version of this article.)

During the tests, the model was towed with an elastic suspension system using a triangular towing arrangement. The longitudinal motions were restricted by a spring in front of and a counter weight behind the model. The suspension system was connected with the ship models by a thin elastic cross bar, which was mounted on deck of the aft segment. With this arrangement, heave and pitch motions remain unrestrained. For this investigation, the LNGC was placed in such a way in the wave tank that the highest waves of the Peregrine breather occur at the forward perpendicular.

3.4. New Year Wave

For the evaluation of breather-type abnormal waves being applicable as design abnormal waves the famous NYW was chosen for the purpose of comparison. This giant single wave (H_{max}=25.63 m) with a crest height of H_c=18.5m has been recorded during a storm on January 1, 1995 at the Draupner platform in the North Sea, (Haver and Anderson, 2000) and occurred in a surrounding sea state characterized by a significant wave height of H_s=11.92 m (H_{max}/H_s=2.15) at a water depth of d=70 m.

The reproduction of such complex structures require sophisticated optimization procedures. To transfer the recorded NYW into the wave tank, an optimization approach for the experimental generation of tailored wave sequences with predefined characteristics has been used (Clauss and Schmittner, 2005). This method enables the generation of scenarios with a single high wave superimposed to irregular seas. During the experimental optimization special emphasis is laid on the exact reproduction of the wave height, crest height, wave period as well as the vertical and horizontal asymmetry of the target wave. Real-world nonlinear free surface effects are included in the optimization procedure, since the procedure is executed by physical wave tank experiments. Fig. 3 presents the reproduced NYW registered in the wave tank in comparison to the original wave sequence recorded at the Draupner platform.

4. Abnormal wave investigation

The starting point was the definition of carrier wave lengths of the Peregrine solution to be of interest for the subsequent wave-structure investigations. The carrier wave lengths were chosen based on the vertical bending moment response amplitude operator (RAO) which represents the linear response due to excitation at a certain wave frequency. With regard to the vertical bending moment, the maximum of the RAO is located at wave lengths which equal ship length. Based on this approach, four the carrier wave lengths were chosen for the generation of breather-type abnormal waves based on the Peregrine solution (Eq. (3)). Table 2 gives an overview on the investigated carrier wave length in terms of wave length (L_w) to ship length between

Table 1
Main dimensions of the investigated LNGC.

	Length [m]	Breadth [m]	Draft [m]	Displacement [t]	Block coefficient [dimensionless]	Speed (knots)
LNGC	186.9	30.4	8.4	35675	0.75	0

perpendicular (L_{pp}) ratio.

The four Peregrine breathers were generated in such a way that the high single wave at target location is as high as physically possible for the defined wave lengths. To arrive at a specific wave height, the initial wave steepness at the wave board is the decisive parameter which was adjusted in such a way that the steepness of the three times higher exaggerated target wave was within the breaking regime. The experiments showed that waves of initial steepness $\epsilon=a_0k_0\leq0.1$ do not break (cf. Chabchoub et al., 2012; Slunyaev et al., 2013; Onorato et al., 2013). Larger steepness resulted in wave breaking of spilling type and became plunging type as the initial wave steepness has been further increases. The generation of breaking abnormal waves allows investigating the impact on offshore structures and ship not only in terms of global loads but also in terms of local loads (e.g. slamming, green water). Target location denotes the location of the subsequent wave-structure investigations, which was approximately x=45 m in front of the wave maker. The model was placed in such a way that the target wave reaches its maximum wave height at the forward perpendicular.

Fig. 4 presents the measured Peregrine breathers at the moment of abnormal wave occurrence at target location. Each breather evolved to high, steep single waves, i.e. increased with increasing carrier wave length – the corresponding wave heights are presented in Table 2 (maximum wave height H_{max}, maximum wave crest height $H_{C_{max}}$ and maximum wave trough height $H_{t_{max}}$). The four breathers' arrived at impressive (zero-upcrossing) wave steepness' ($\epsilon=\pi H/L=0.38\ldots0.42$) being plunging breakers close to the target location. The upcrossing wave periods of the individual abnormal waves were approximately one second shorter than the (input) carrier periods of the surrounding waves. However, Fig. 4 proves that the Peregrine breather solution can be used for systematic abnormal wave generation of certain frequency.

Analysing the measured maximum wave height and crest height, respectively, reveals that the Peregrine IV breather reached almost the same crest height and a significant higher overall wave height compared to the NYW (Table 2, cf. Chabchoub et al., 2010). Fig. 5 compares the reproduced NYW (blue curve) and the Peregrine IV breather (red curve) showing that the Peregrine breather features a similar abnormal wave characteristic. However, the Peregrine breather is also characterized by deeper preceding and succeeding troughs as well as shorter up- and downcrossing wave periods, i.e. this Peregrine breather is higher and steeper compared to the NYW.

In the next step, the wave characteristics are analysed in terms of dynamic pressure and horizontal particle velocity for the two abnormal waves shown in Fig. 5. Fig. 6 presents coloured parametric surface plots of the measured horizontal velocities under the Peregrine breather (top) and the NYW (bottom). Both diagrams show the same trend – the highest horizontal particle velocities are observed under the deepest wave troughs and highest wave crests, respectively. The velocities under the target wave crests are reaching the highest values for both wave sequences.

Table 2
Main characteristics of theabnormal waves at target location.

Wave	$\frac{L_w}{L_{PP}}$	H_{max} (m)	Hc_{max} (m)	Ht_{max} (m)
Peregrine I	0.7	12.82	8.29	4.53
Peregrine II	0.9	16.2	11.17	5.03
Peregrine III	1.1	21.73	14.87	6.86
Peregrine IV	1.3	28.86	18.64	10.22
New Year Wave	1.3	26.93	18.76	8.17

The associated coloured parametric surface plots of the measured dynamic pressure are shown in Fig. 7 – top for the Peregrine breather and bottom for the NYW. Comparing the dynamic pressure reveals the same trend – the highest/lowest dynamic pressures can be observed under the highest wave crests and deepest wave troughs, respectively. Again, the dynamic pressures under the target wave crests are reaching the highest values for both wave sequences.

For the purpose of comparison, the pressure as well as the velocity profile under the abnormal waves (maximum surface elevation) are presented in Fig. 8. The left diagram shows the horizontal velocity profiles under the NYW crest (blue dots) and the Peregrine breather wave crest (red dots), and the right diagram the corresponding dynamic pressure profiles. The velocity profiles near the surface area (up to z≈−30 m) feature almost the same characteristic and diverge with increasing water depth, i.e. the Peregrine breather reaches lower horizontal velocities near the bottom compared to the NYW. The dynamic pressure illustrates almost the same trend, even if both profiles do not overlap in the course of the upper half, a distinctive discrepancy at the deepest measured position can be observed. The reason for the difference lies in the different wave lengths as discussed before, the effect of kinematics and dynamics decreases faster for the shorter Peregrine breather. However, both abnormal waves feature a similar characteristic near the surface area.

Based on the results presented above, which prove that the breather solutions represent a promising alternative to real-world abnormal wave investigations in terms of model tests, an extract of a Peregrine breather was integrated into an irregular sea state to exploit the application spectrum of breather solutions in terms of tailoring deterministic irregular sea states with embedded abnormal waves. This extract was identified by preceding experimental investigations. On one hand, the preceding investigations focussed on the identification of a Peregrine breather solution which features a similar wave characteristic in terms of crest height and shape of the abnormal wave at target location (maximum amplification) compared to the NYW (cf. Fig. 5). On the other hand, based on the identified solution, the number of background waves in front of and behind the perturbation were iteratively reduced to identify the minimum number of background waves necessary to trigger modulation instability reaching the same

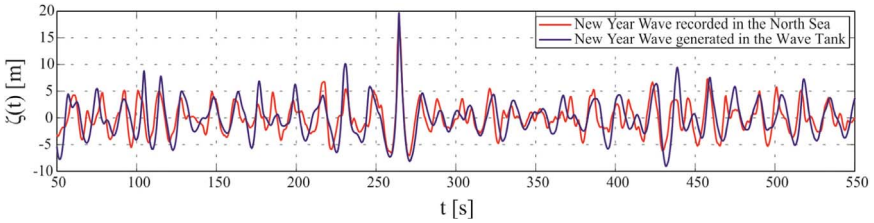

Fig. 3. Comparison of reproduced model wave train at target location and the sequence recorded at the Draupner platform.

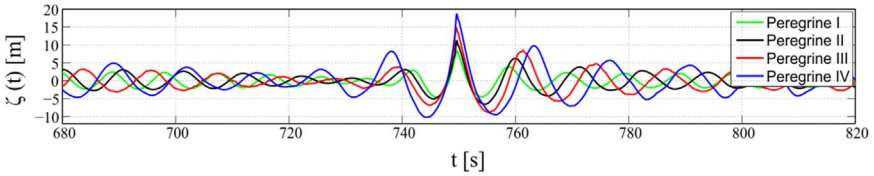

Fig. 4. Comparison of the four investigated Peregrine breather measured at target location. The measured surface elevations are shifted in time domain for a better comparability.

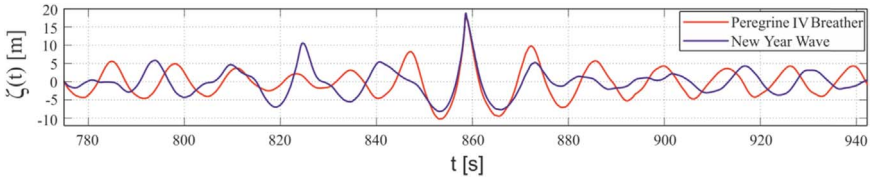

Fig. 5. NYW vs. Peregrine Breather: Comparison between real-world NYW reproduction and Peregrine IV breather measured at target location. The measured surface elevations are shifted in time domain for a better comparability. (For interpretation of the references to color in this figure legend, the reader is referred to the web version of this article.)

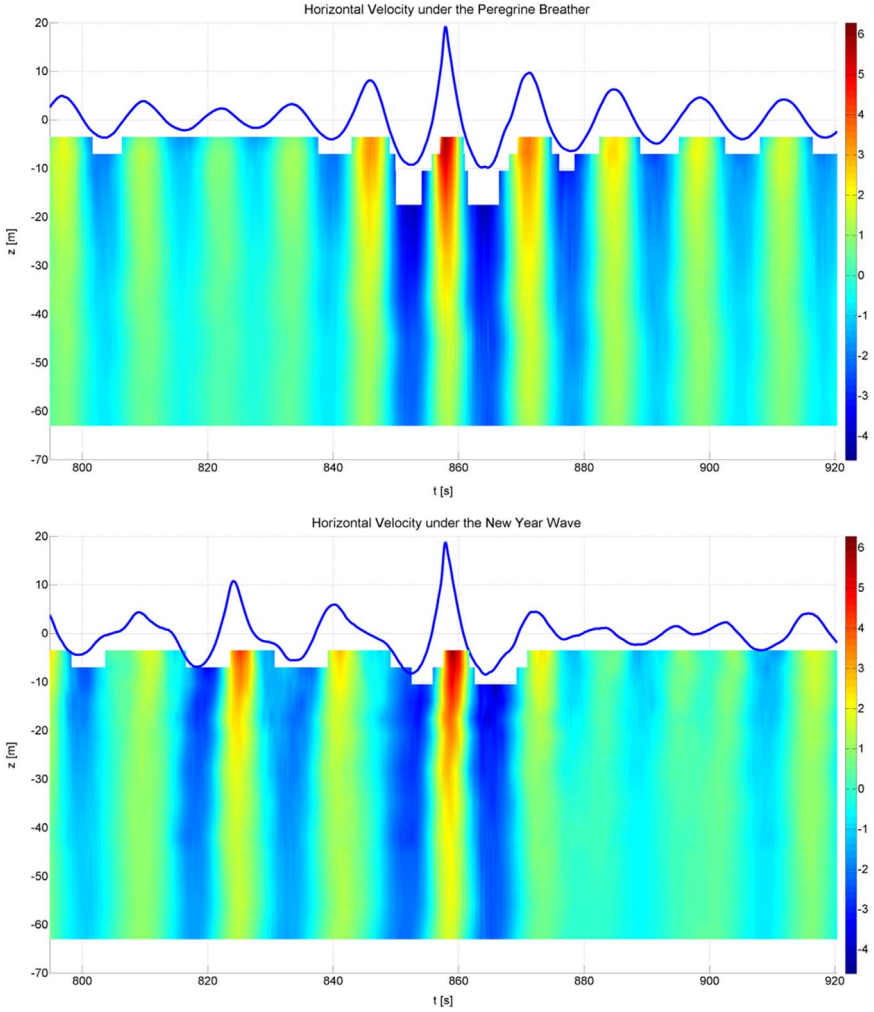

Fig. 6. Horizontal particle velocity field [m/s] under the Peregrine IV breather (top) and the NYW (bottom) in full scale. (For interpretation of the references to color in this figure legend, the reader is referred to the web version of this article.)

abnormal wave compared to the basic solution. For the irregular sea state part, the real-world NYW registered at the Draupner platform were used as basis. A segment of t=125 s around the NYW was removed from the registration by what two separate irregular sea segments were left over. These segments are afterwards linearly transformed back to the position of the wave maker. At the end, the three wave segments at the wave board (irregular sea in front of the breather, breather and the irregular sea after the breather) were connected in such a way that the irregular waves surround the breather but the breather itself was undisturbed from it at the beginning of the wave evolution (cf. Fig. 9 top). This simple procedure was applied to reproduce the NYW with a Peregrine breather such as shown in Fig. 5 by taking irregular waves in front of and behind the target wave into account.

Fig. 9 presents the experimental results. The top diagram shows the determined wave board motion. The extract of the Peregrine breather is

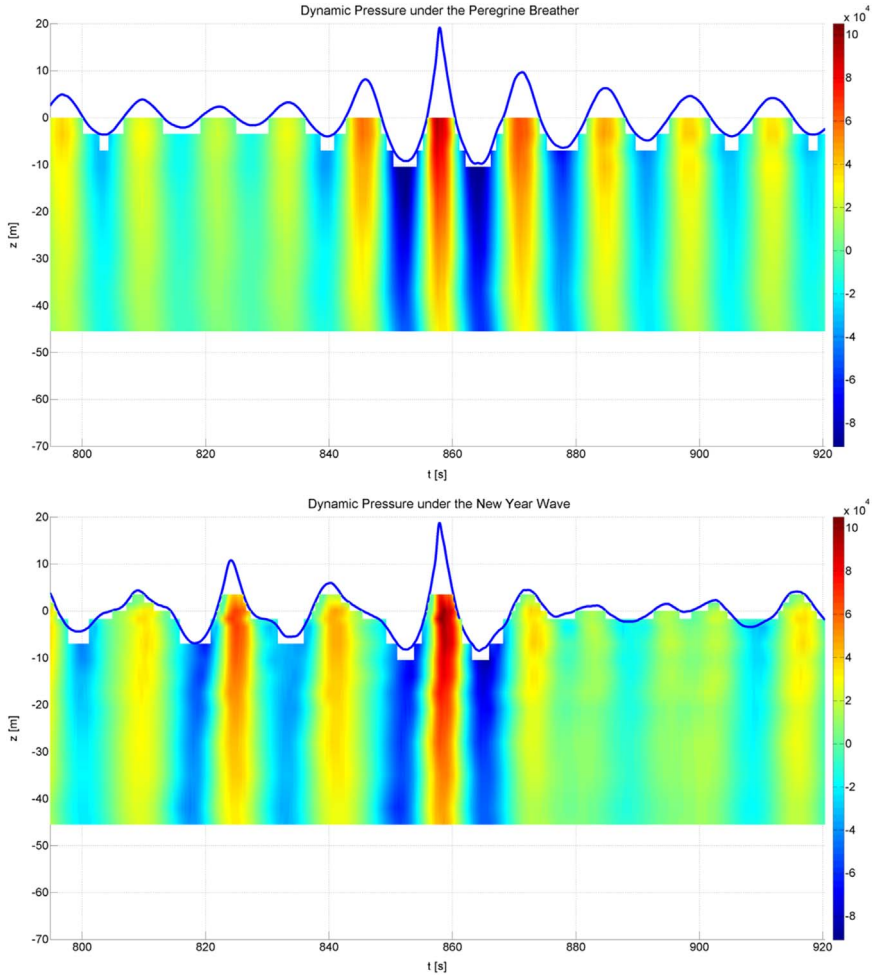

Fig. 7. Dynamic pressure field [Pa] under the Peregrine IV breather (top) and the NYW (bottom) in full scale.

obviously. The second and third diagram from top illustrates the measured surface elevation at x=10 m and x=50 m in front of wave maker, respectively. The Peregrine solution provides already a high single wave within the breather sequence at the wave board due to the short distance between wave maker and target location. At the target location, the high single wave reaches its maximum wave height and the surrounding waves merge to an irregular wave shape. The bottom diagram compares the tailored irregular sea state with embedded Peregrine breather with the NYW. This proves that breather solutions are capable to tailor irregular sea states including a high single wave as well as that the solutions can be applied for the generation of realistic irregular wave environments.

5. Abnormal wave-structure investigation

So far, the characteristics of breather solutions are evaluated and compared to the real-world NYW. Following, their impact on offshore structures in terms of forces and motions relevant for the design is addressed. Experimental as well as numerical investigations in the four Peregrine breather presented above (cf. Table 2) are compared to results in the NYW.

In the numerical model, the LNGC was divided into 34 stations and each station was further divided into 20 segments of equal length. Table 3 shows the location of the stations from the aft perpendicular (AP) and Fig. 10 shows the body plan of the ship. The numerical integration of the equation of motion (Eqs. (8)–(10)) was carried out using implicit trapezoidal method with a time step of 0.1 s. The experimental incident waves served as inputs for the numerical simulation. The harmonics were calculated from the Fourier transform of the wave time series measured in the wave tank at amidships of the LNGC, i.e. the evolved waves directly behind the target location. The numerical wave elevation in space domain was calculated from the harmonics using Eq. (11) based on the linear dispersion relationship. Even though the numerical simulation uses the nonlinear wave profile that was measured during the model test at amidships, the calculated pressure under the wave profile was still linear and the nonlinear wave propagation was not considered which is beyond the scope of study. Other aspects, such as green water shipping and slamming, which can also influence the ship responses in severe seas, were not investigated.

Fig. 11 shows the direct time series comparison of the numerical and the measured incident waves, heave and pitch motions and the vertical bending moment at amidships in breather-type abnormal waves and in NYW. The solid lines represent experimental results and numerical results are shown by the dotted lines. The acronyms ‘Exp’ and ‘TDNL’ , respectively, denote the experimental and the numerical results. The positive heave and pitch values, respectively, indicate the ship emergence and bow down conditions and the positive bending moment shows the hogging condition. The numerical and the measured incident waves at amidships coincide exactly with each other for all the tested cases as the measured waves are used for the numerical simulation. Regarding the heave motions, the agreement between the measured and the numerical results are good in general; however, the positive heave peaks are slightly overestimated by the numerical methods. The positive heave value shows the ship emergence. This can be partly due the viscous effects and the associated flow separation that occurs under the flat bottom and the bow flare region

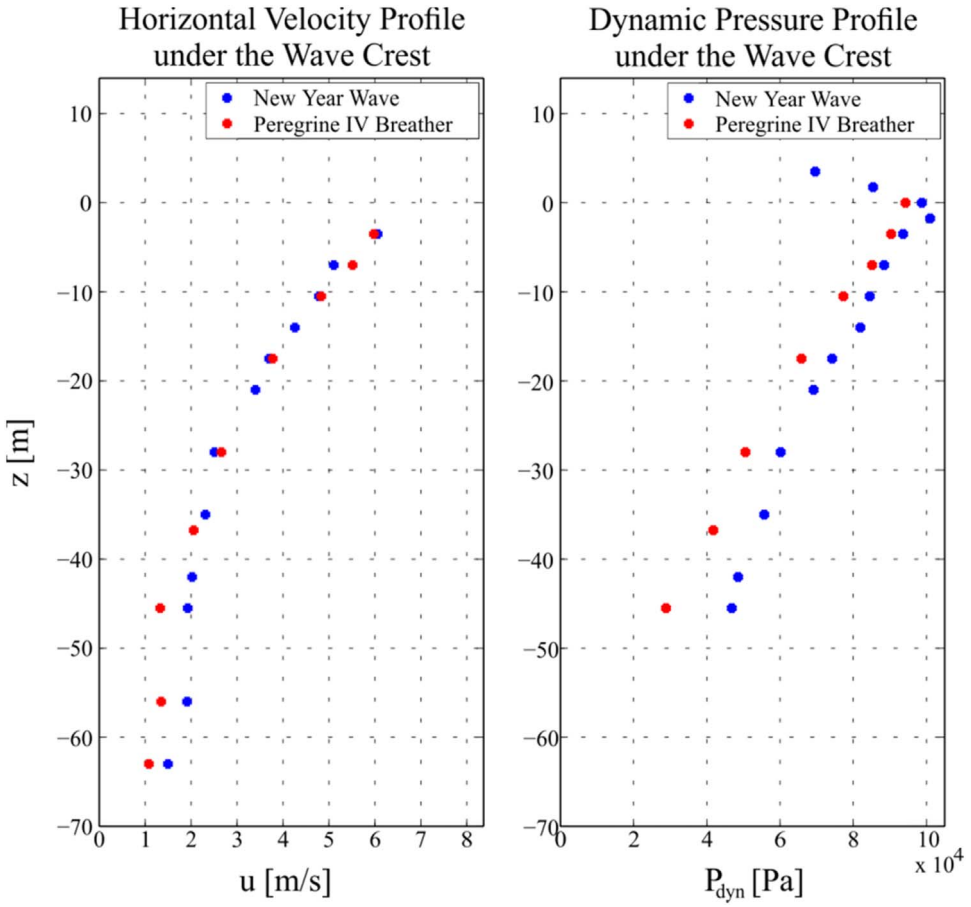

Fig. 8. Horizontal velocity (left) and dynamic pressure (right) profile under NYW crest and Peregrine breather wave crest (full scale).

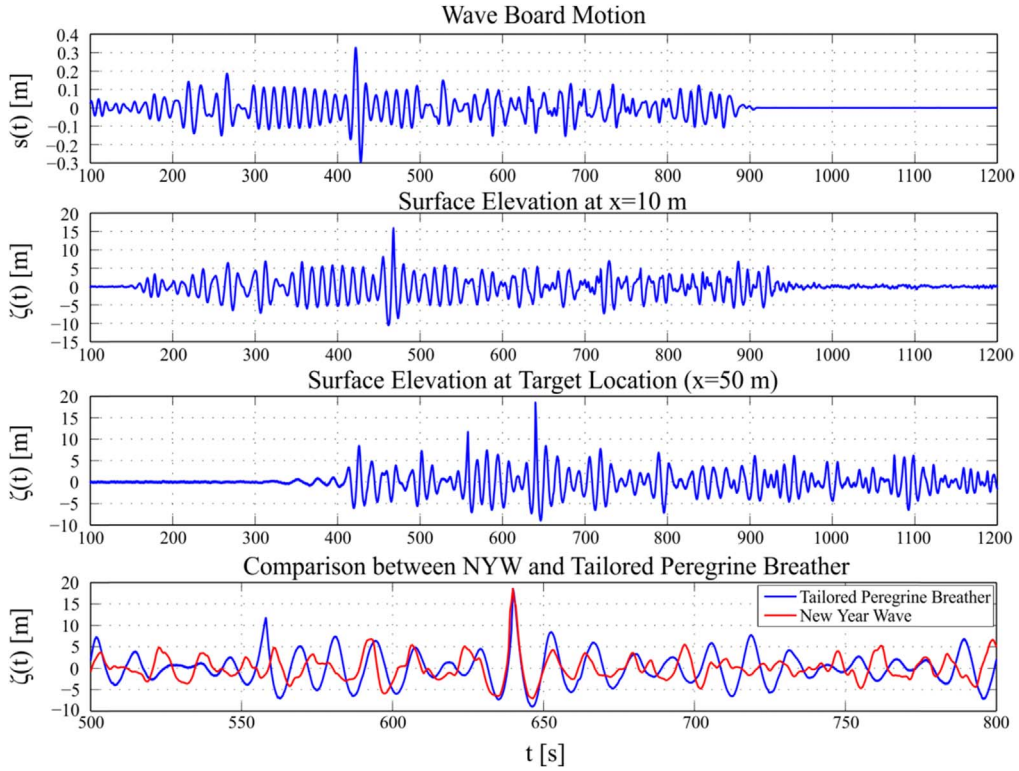

Fig. 9. Generation of a tailored Peregrine breather – integration of a Peregrine Breather into an irregular sea state.

Table 3
Location of the station from the aft perpendicular (AP).

Station	AP1	AP	1	2	3	4	5	6	7	8	9	10	11	12	13	14	15	16	17
Distance from AP (m)	−3	0	4	6	8	12	16	20	24	32	40	48	56	64	72	80	88	93.45	104
Station	18	19	20	21	22	23	24	25	26	27	28	29	FP	FP1	FP2				
Distance from AP (m)	112	120	128	136	144	152	160	168	172	176	180	184	186.90	188	190				

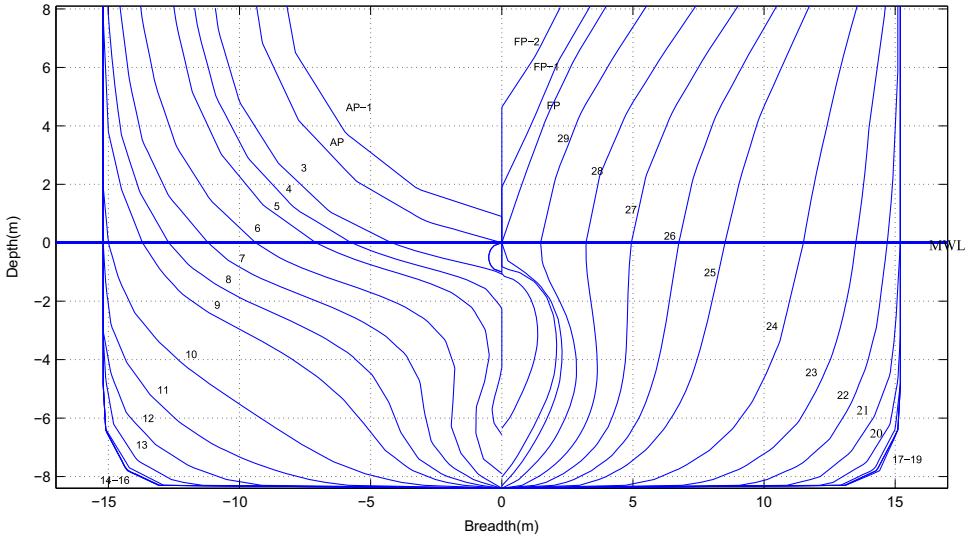

Fig. 10. Body plan of the LNGC.

when the ship hull moves up in very large amplitude waves. Beukelman (1983) showed that the drag coefficient is a function of the frequency and the free surface waves influence the vortex shedding in the vertical response of the ships. The pitch motions are better calculated by the numerical method and the calculated vertical bending moments are in very good agreement with the measured ones.

Rajendran et al. (2015a) presented the heave and pitch response of a cruise vessel in large amplitude waves observing similar response where the ship emergence and bow up condition is overestimated by the numerical method. However, on further investigation it has been found that the experimental incident wave field around the hull is distorted due to radiated and diffracted waves. In order to check the effect of distorted wave field on the ship motions, a heuristic approach was used to modify the numerical incident wave so that it matches with the measured incident wave. This approach significantly improved the prediction of the heave and pitch responses.

Apart from the aforementioned viscous effects, other nonlinear phenomena such as nonlinear wave propagation, nonlinear wave pressure, green water load and slamming can also play an important role in the discrepancy between the numerical and the measured responses. Even though, the numerical simulations used experimental nonlinear wave profile, linear dispersion was used for the distribution of the wave profile along the length of the ship. Nonlinear wave propagation is beyond the scope of the present seakeeping method since the method has been designed for estimation of the long term distribution of loads, which requires that the method is fast and accurate enough for practical engineering applications. Moreover, the calculated pressure under the waves is still linear. Green water load calculation based on momentum theory, demands a good estimation of the nonlinear wave profile and the relative motion of the ship in order to calculate the exact height of the green water above the deck. This is certainly beyond the scope of the present study. Whipping load was not considered in the study assuming that slamming and associated whipping response has little effect on the rigid body motions and loads. However, it could be seen from the results that one of the main sources of nonlinearity is associated with the geometry of the ship, which the method is able to take into account.

The probability of exceedance of the peaks of the numerical and the experimental incoming NYW and the associated ship responses are shown in Fig. 12. The tests are conducted for 20 min which consisted of 90 wave cycles. Since the tests were not repeated, statistical uncertainty in the distribution of the peaks due to the limited data is expected. This could be observed from the spreading of the response peaks at the tail of the distribution. However, since one of the main objectives of the study is direct comparison of the extreme peaks of the numerical and the experimental time series, probability distribution serve as a supplement to see the correlation between the numerical and the measured peaks for the rest of the time series. The circle and the diamond symbols represent the positive and negative peaks of the experimental results and the solid line and the line with '+' marks show the positive and negative numerical peaks. Both the numerical and the measured wave peaks at amidships coincide with each other. The asymmetry in the distribution of the incident wave peaks, with the crests peaks being larger than the trough peaks, clearly shows the nonlinearity associated with the waves. The measured positive and negative heave peaks are only slightly asymmetric except at the tail of distribution and the ship submerges more and emerges less. The numerical simulation is able to capture the ship submergence well, however it overestimates the emergence. The aforementioned flow separation associated with the ship emergence in high seas, which is not taken into account in the potential flow method, and the dynamic swell up can be a possible reason behind the measured lower emergence.

Similar to the heave response, the experimental pitch is only slightly asymmetric except at the tail of the distribution. Pronounced bow flares acts as a strong source of nonlinearity due to the reserve

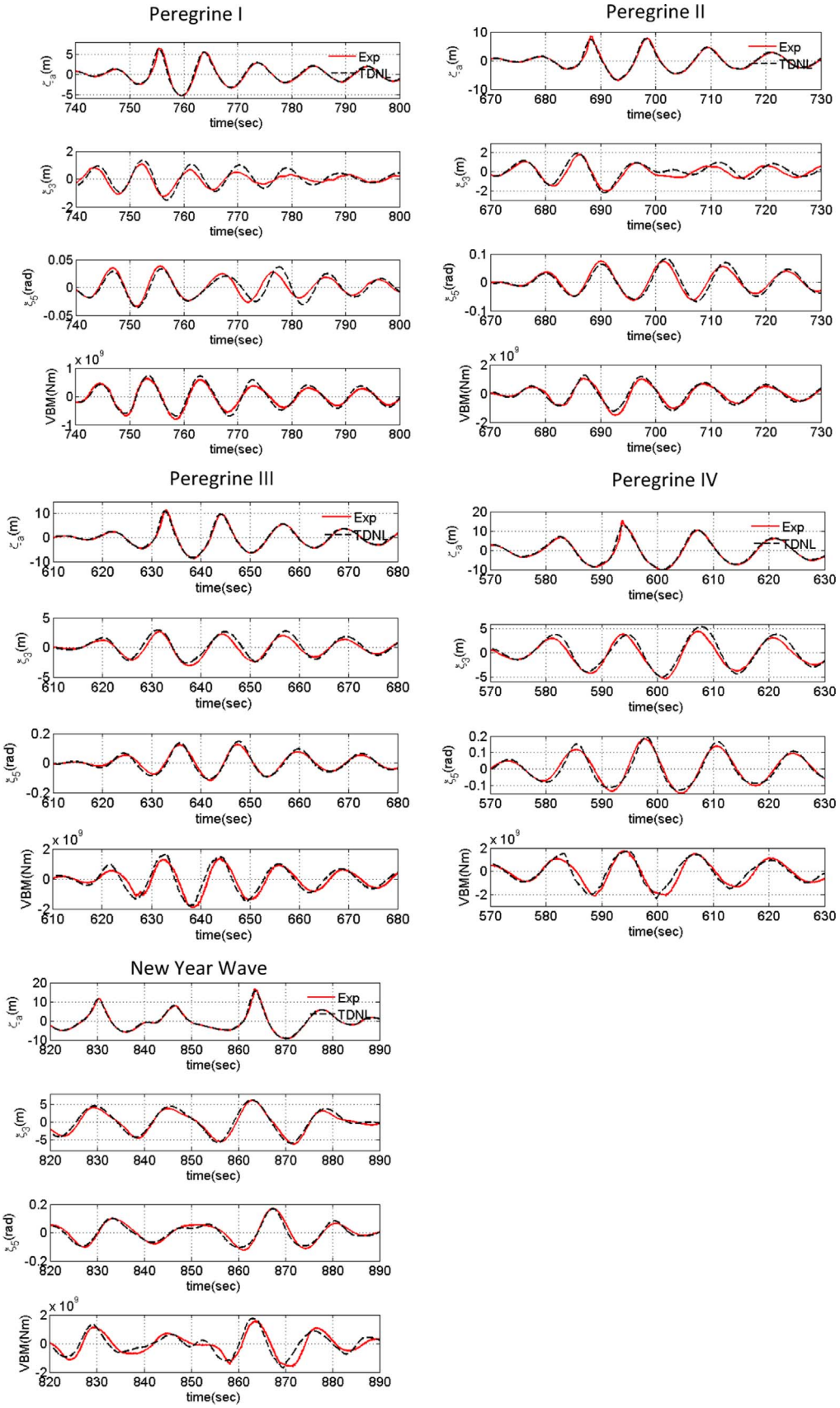

Fig. 11. Time series comparison of the measured and the numerical incident wave elevations, heave and pitch and the vertical bending moment at amidships.

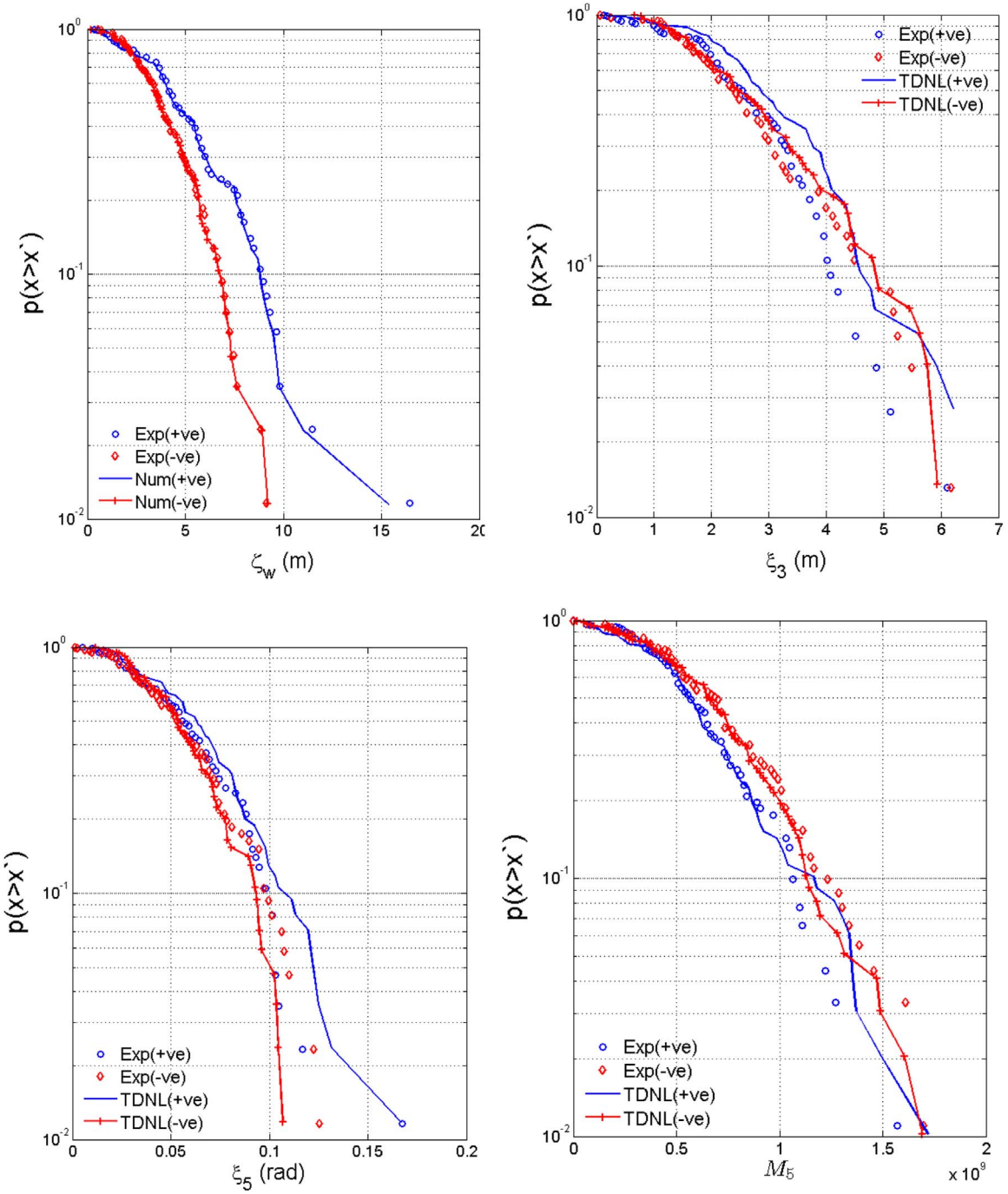

Fig. 12. Probability of exceedance of the peaks of the measured and the numerical incident wave elevations, heave and pitch and the vertical bending moment at amidships.

buoyancy and nonlinear hydrodynamic disturbance generated in the bow region (Watanabe et al., 1989). However, unlike the containership models tested by Fonseca and Guedes Soares (2004), the pitch peaks of LNGC do not show any strong nonlinearity even in extreme seas. This is due to the fuller body of the LNGC (C_B=0.75) and lower bow flare angle with respect to the containership (C_B=0.64). The pitch peak data at the tail of the distribution is scattered, however the distribution of the peaks provides a fair insight into the behaviour of the ship in abnormal waves, even though a larger number of wave cycles would reduce the statistical uncertainty. The ship bow submerges slightly more than it rises, which can also be due to flow separation under the bottom and the bow during the bow emergence. The numerical results follow the measured responses, both qualitatively and quantitatively.

Fig. 12 also present the distributions of the vertical bending moment peaks at amidships. The peaks are asymmetrically distributed with larger sagging peaks and smaller hogging peaks and the numerical results are able to predict the vertical bending moment of the ship accurately. At the tail of the distribution, the hogging peaks are slightly overestimated by the numerical results.

Finally, the largest sagging and hogging values in the Peregrine IV breather and the NYW are shown in Table 4 and compared with the IACS Common Structural Rules for Bulk Carriers and Oil Tankers (2015). Even though the simulation run was limited to 20 min for the cases analysed in the paper, it was assumed that the chance to generate another huge wave is very small if the simulation run has been extended to 3 h. It is also a known fact the ship loads are strongly influenced by the length of the encountering waves. Therefore, the test was conducted for a range of wave to ship length ratio varying between

Table 4
Rule bending moment vs. measured and numerical vertical bending moment.

	Rule bending moment	Experiment	Numerical
Hogging (10^9) N m- New Year wave	1.73	1.61	1.73
Sagging (10^9) N m-New Year wave	1.94	1.73	1.71
Hogging (10^9) N m- Peregrine IV	1.73	1.78	1.71
Sagging (10^9) N m- Peregrine IV	1.94	2.12	2.34

0.7 and 1.3. Therefore, it is assumed that the wave load experienced by the ship in these abnormal waves will be the largest one during its life cycle. Presently, the abnormal waves are not accounted for the ship structural design rules. Therefore, it is not necessary that the present design loads are able to cover the maximum vertical bending moment under abnormal waves. The rule values of the sagging and hogging moments are the expected maximum values during the lifetime of the ships. However, the numerical values discussed in the following sections are the maximum values during an event, when the ship encounters the abnormal waves. Therefore, the rule values are considered here as a reference to discuss the relative magnitude of VBM. The maximum hogging and sagging loads experienced by the LNGC in the Peregrine IV breather are slightly larger than the maximum loads in the NYW due to the difference of the wave characteristics in front of and behind the extraordinarily large wave crest (cf. Fig. 5). The Peregrine IV breather features a more critical characteristic in terms of wave length and height particularly in front of the abnormal wave crest. In addition, breather solutions feature a symmetrical shape around the abnormal wave crest resulting in an experimental design abnormal wave whose critical wave length can be adjusted precisely. They prove to be a very good tool for the estimation of the design loads representing outstanding critical wave events in terms of structure response. The rule bending moment is able to cover the largest bending moment experienced by the LNGC in the NYW. The percentage of error between the measured and the numerically calculated values for the given cases is always less than 10%.

6. Conclusions

This paper introduces breather solutions of the NLS equation, namely the Peregrine solution, as an innovative design abnormal wave for abnormal wave-structure investigations. Thereby, the characteristics of the Peregrine breather as well as their impact on a LNGC are addressed. For the purpose of comparison, the real-world NYW is additionally investigated allowing the evaluation of breather-type abnormal waves in terms of applicability as design abnormal wave.

The investigations on abnormal wave characteristics demonstrates that the Peregrine breather solution can be used for systematic abnormal wave generation of certain frequency, i.e. abnormal waves up to the maximum possible wave height are generated for predefined critical wave lengths. In addition, it is shown that the breather-type abnormal waves feature a similar abnormal wave characteristic compared to the real-world NYW. Moreover, the potential span of application has been demonstrated by integrating a breather solution into an irregular sea state resulting in an abnormal wave within a random wave field. Altogether, this investigation verifies that the breather solutions are applicable for the deterministic generation of tailored extreme waves.

The application of breather solutions to abnormal wave-structure interaction is investigated by experiments and numerical simulations. Again, Peregrine breathers as well as the NYW are considered. Evaluating the structure response reveals that the impact of the abnormal waves (Peregrine IV and NYW) is severe resulting in extreme values for the ship response. From direct time series comparison, it is found that the ship emergence is slightly overestimated by the numerical method. This is probably due to the flow separation at the flat bottom which is not taken into account in the potential flow code. The ship submergence and the pitch motions are well captured by the numerical method. The numerical sagging peaks are in very good agreement with the experimental results, but the hogging peak is slightly overestimated by the numerical method. The probability of the exceedance of the ship responses in the NYW shows that the vertical ship motions are only slightly asymmetric except at the tail of the distribution. The IACS rule bending moment value is able to cover the largest load experienced by the ship in the abnormal waves.

Comparing the largest loads, the structure experienced in the Peregrine breathers and the NYW, it is found that the Peregrine IV breather is more severe due to its critical characteristic in terms of wave length and height particularly in front of the abnormal wave crest. This result does not denote that real-world reproductions are useless for the evaluation of wave-structure interaction as they represent abnormal wave events which happened on sea, excluding any doubt regarding discussions on possible unrealistic, artificial wave sequences. However, the investigations prove that the breather-type abnormal waves are very efficient design abnormal waves to be considered for wave-structure investigations on different subjects, e.g. local and global loads, green water effects as well as air gap investigations. The major benefits are the potential to generate abnormal waves of certain frequency up to the physically possible wave height, the symmetrical shape of the abnormal wave and the availability of an analytical solution.

Acknowledgments

This paper is published as a contribution to the project EXTREME SEAS, which is funded by the European Commission, under the Grant agreement no. 234175. We highly acknowledge the support of this research project and want to thank our project partners Det Norske Veritas AS, Germanischer Lloyd SE, Meteorological Institute, Institute of Applied Physics, Canal de Experiencias Hidrodinamicas de El Pardo, Meyer Werft, Estaleiros Navais Viana de Castelo and University Duisburg-Essen for their contributions.

References

Adegeest, L., Braathen, A., and Vada, T., 2000. Evaluation of methods for estimation of extreme nonlinear ship responses based on numerical simulations and model tests. In: Twenty-Proceedings of the Second Symposium on Naval Hydrodynamics, 84–99. Washington, D.C., USA.

Akhmediev, N., Korneev, V., 1986. Modulation instability and periodic solutions of the nonlinear schrödinger equation. Theor. Math. Phys. 69 (2), 1089–1093.

Akhmediev, N., Eleonskii, V., Kulagin, N., 1985. Generation of periodic trains of picosecond pulses in an optical fiber: exact solutions. Sov. Phys. JETP 62 (5), 894–899.

Akhmediev, N., Eleonskii, V., Kulagin, N., 1987. Exact first-order solutions of the nonlinear Schrödinger equation. Theor. Math. Phys. 72 (2), 809–818.

Akhmediev, N., Ankiewicz, A., Taki, M., 2009a. Waves that appear from nowhere and disappear without a trace. Phys. Lett. A 373 (6), 675–678.

Akhmediev, N., Ankiewicz, A., Soto-Crespo, J.M., 2009b. Phys. Rev. E 80, 026601.

Andonowati, Karjanto, N., Groesen, E.V., 2006. Extreme wave phenomena in down-stream running modulated waves. Appl. Math. Model. 31 (7), 1425–1443.

Beukelman, W., 1983. Vertical Motions and Added Resistance of a Rectangular and Triangular Cylinder in Waves. Ship Hydrodynamics Laboratory: Delft University of Technology.

Bertotti, L., Cavaleri, L., 2008. Analysis of the Voyager storm. Ocean Engineering 35 (1), 1–5.

Buchner, B., 1995. On the Impact of Green Water Loading on Ship and Offshore Unit Design. In: PRADS95–Proceedings of the 6th Symposium on Practical Design of Ships and Mobile Units. Seoul, Korea.

Chabchoub, A., Vitanov, N., Hoffmann, N., 2010. Experimental evidence for breather type dynamics in freak waves. Proc. Appl. Math. Mech. 10, 495–496. http://dx.doi.org/10.1002/pamm.201010240.

Chabchoub, A., Hoffmann, N., Akhmediev, N., 2011. Rogue wave observation in a water wave tank. Phys. Rev. Lett. 106, 20.

Chabchoub, A., Akhmediev, N., Hoffmann, N.P., 2012. Experimental study of spatiotemporally localized surface gravity water waves. Phys. Rev. E 86 (1), 06311.

Clauss, G.F. and Kühnlein,W., 1996. Nonlinear Transient Wave Excitation as a new Tool in Model Testing. International Conference on Ocean, Offshore and Arctic Engineering. Florence, Italy. OMAE 96–552.
Clauss, G.F. and Schmittner, C.E., 2005. Experimental Optimization of Extreme Wave Sequences for the Determinisitic Analysis of Wave/Structure Interaction. in: OMAE 2005–Proceedings of the 24th International Conference on Offshore Mechanics and Arctic Engineering. Halkidiki, Greece. OMAE2005-67049.
Clauss, G.F., Schmittner, C.E., and Klein, M., 2006. Generation of Rogue Waves with Predefined Steepness. In: OMAE 2006-Proceedings of the 25th International Conference on Offshore Mechanics and Arctic Engineering. Hamburg, Germany, OMAE2006-92272.
Clauss, G.F., Haver, S.K., and Strach, M., 2010a. Breaking wave Impacts against Platform Columns: Stochastic Analysis and DNV Recommended Practice. In: OMAE2010–Proceedings of the 29th InternationalConference on Ocean, Offshore and Arctic Engineering. Shanghai, China. OMAE2010-20293.
Clauss, G.F., Klein,M., and Dudek, M., 2010b. Influence of the Bow Shape on Loads in High and Steep Waves. in: OMAE 2010–Proceedings of the 29th InternationalConference on Offshore Mechanics and Arctic Engineering. Shanghail, China. OMAE2010-20142.
Clauss, G.F., Dudek, M., and Klein, M., 2011a. Influence of Wave Group Characteristics on Loads in Severe Seas. In: OMAE2011–Proceedings of the 30th InternationalConference on Ocean, Offshore and Arctic Engineering. Rotterdam, The Netherlands. OMAE2011-49940.
Clauss, G.F., Klein, M., and Onorato, M., 2011b. Formation of Extraordinarily High Waves in Space and Time. In: OMAE 2011–Proceedings of the 30th InternationalConference on Ocean, Offshore and Arctic Engineering. Rotterdam, The Netherlands. OMAE2011-49545.
Clauss, G.F.,Klein, M., Dudek, M., and Onorato, M., 2012. Application of Breather Solutions for the Investigation of Wave/Structure Interaction in High Steep Waves. OMAE 2012–31th International Conference on Ocean, Offshore and Arctic Engineering. Rio de Janeiro, Brazil. OMAE2012-83244.
Clauss, G.F., Klein, M., Guedes Soares, C., Fonseca, N., 2013. Response based identification of critical wave scenarios. J. Offshore Mech. Arct. Eng.. http://dx.doi.org/10.1115/1.4024269.
Clauss, G.F., Schmittner, C.E., Hennig, J., Guedes Soares, C., Fonseca, N. and Pascoal, R., 2004.Bending Moments of an FPSO in Rogue Waves. In: OMAE–Proceedings of the 23rd InternationalConference on Offshore Mechanics and Arctic Engineering. Vancouver, Canada. OMAE2004-51504.
Dietz, J.S., 2004. Application of conditional waves as critical wave episodes for extreme loads on marine structure. Tech. Univ. Den. Dep. Mech. Eng..
Dubard, P., Gaillard, P., Klein, C., Matveev, V.B., 2010. Eur. Phys. J. Spec. Top. 185, 247.
Dysthe, K.B.,1979. Note on a modification to the nonlinear Schrdinger equation for application to deep water waves. In: Proceedings of the Royal Society of London, Series A369,105–114.
Dysthe, K.B., Trulsen, K., 1999. Note on breather type solutions of the nls as models for freak-waves. Physica Scr. T82, 48–52.
Faulkner, D., Buckley, W.H., 1997, Critical Survival Conditions for Ship Design, International Conference on Design and Operation for Abnormal Conditions, RINA, paper no. 6, pp. 1–25.
Fonseca, N., Guedes Soares, C., 2004. Experimental investigation of the nonlinear effects on the statistics of vertical motions and loads of a container ship in irregular seas. J. Ship Res. 48 (2).
Fonseca, N., Guedes Soares, C., Pascoal, R., 2006. Structural loads induced in a containership by abnormal wave conditions. J. Mar. Sci. Technol. 11, 245–259.
Fonseca, N.; Guedes Soares, C., and Pascoal, R. 2007. Influence of FPSO Length on the Global Loads Induced by Abnormal Waves. In: Proceedings of the 10th International Symposium on Practical Design of Ships and Other Floating Structures (PRADS 2007); Houston, Texas, United States of America. USA: American Bureau of Shipping.
Fonseca, N., Pascoal, R., Guedes Soares, C., 2008. Global structural loads induced by abnormal waves and design storms on a FPSO. J. Offshore Mech. Arct. Eng. 130, 021005–1/021005-9.
Fonseca, N., Pascoal, R., Guedes Soares, C., Clauss, G.F., Schmittner, C.E., 2010. Numerical and experimental analysis of extreme wave induced vertical bending moments on a FPSO. Appl. Ocean Res. 32 (374–390), 148–167.
Friis-Hansen, P. and Nielsen,L.P., 1995. On the New Wave Model for the Kinematics of Large Ocean waves. In: OMAE 1995–Proceedings of the 14th International Conference on Offshore Mechanics and Arctic Engineering. Copenhagen, Denmark.
Gaillard, P., 2012. J. Math. Sci.: Adv. Appl. 13, 71.
Gorf, P., Barltrop, N., Okan, B., Hodgson, T., Rainey, R., 2000. FPSO Bow Damage in Steep Waves. Rogue Waves 2000, Brest, France.
Groesen, E.V., Andonowati, A., Karjanto, N., 2006. Displaced phase-amplitude variables for waves on finite background. Phys. Lett. A 354 (4), 312–319.
Guedes Soares, C., Fonseca, N., Pascoal, R., 2008. Abnormal wave induced load effects in ship structures. J. Ship Res. 52 (1), 30–44.
Guedes Soares, C., Pascoal, R., Antao, E., Voogt, A., Buchner, B., 2007. An approach to calculate the probability of wave impact on a FPSO Bow. J. Offshore Mech. Arct. Eng. 129 (2), 73–80.
Guedes Soares, C., Fonseca, N., Pascoal, R., Clauss, G.F., Schmittner, C.E., Hennig, J., 2006. Analysis of design wave loads on a FPSO accounting for abnormal waves. J. Offshore Mech. Arct. Eng. 128 (3), 241–247.
Haver, S. and Anderson,O.J., 2000. Freak waves: rare realization of a typical population or typical realization of a rare population? In: Proceedings of the 10th International Offshore and Polar Engineering Conference (ISOPE). Seattle, USA.
Henderson, K.L., Peregrine, D.H., Dold, J.W., 1999. Unsteady water wave modulations: fully nonlinear solutions and comparison with the nonlinear Schrödinger equation. Wave Motion. http://dx.doi.org/10.1016/s0165-2125(98)00045-6.
Huijsmans, R.H.,M., Klopman, G., KarjantoN., and Andonawati, 2005. Experiments on extreme wave generation using the Soliton on Finite Background. ArXiv e-prints. Ifremer, Brest, France.
IACS Common Structural Rules for Bulk Carriers and Tankers, 2015
Karjanto, N. and Groesen, E.V., 2007. Derivation of the NLS breather solutions using displaced phase-amplitude variables. In: Proceedings of SEAMS-GMU Conference.
Karunakaran, D., Baerheim, M., and Leira, B.J., 1997. Measured and simulated dynamic response of a jacket plattform. In: Proceedings of the 16th InternationalConference on Offshore Mechanics and Arctic Engineering, Vol. II. Yokohama, Japan
Kharif, C., Pelinovsky, E., Slunyaev, A., 2009. Rogue Waves in the Ocean. Springer-Verlag Berlin Heidelberg.
Klein, M., 2015. Tailoring Critical Wave Sequences for Response-based design, in Dissertation. Technische Universität Berlin.
Kuznetsov, E., 1977. Solitons in a parametrically unstable plasma. Akad. Nauk SSSR Dokl. 236, 575–577.
J. Lemire Freak wave rocks cruise 2005. < http://www.nydailynews.com/archives/news/freak-wave-rocks-cruise-70-footer-hits-n-y-bound-ship-article-1.622703. >
Ma, Y., 1979. The perturbed plane-wave solutions of the cubic Schrödinger equation. Stud. Appl. Math. 60, 43–58.
Mei, C.C., 1989. The applied dynamics of ocean surface waves. Advanced Series on Ocean Engineering - Volume 1, World Scietific Publishing Co. Pte. Ltd., 5 Toh Tuck Link, Singapore 596224. 1.
Mori, N., Yasuda, T., and Nakayama, S. in: , 2000, Statistical properties of freak waves observed in the Sea of Japan. In: Proceedings of the Tenth International Offshore and Polar Engineering Conference (ISOPE), Vol. 3. Seattle, WA, pp. 109–122.
Onorato, M., Proment, D., Clauss, G., Klein, M., 2013. Rogue waves: from Nonlinear Schro¨ dinger Breather Solutions to Sea-Keeping Test. PLoS One 8 (2), e54629. http://dx.doi.org/10.1371/journal.pone.0054629.
Osborne, A.R., Onorato, M., Serio, M., 2000. The nonlinear dynamics of rogue waves and holes in deep-water gravity wave trains. Phys. Lett. A 275, 386–393.
Pastoor W., Helmers JB, Bitner-Gregersen E. 2003. Time simulation of ocean going structures in extreme waves. In: Proceedings of the 22th International Conference on Offshore Mechanics and Arctic Engineering. Cancun, Mexico. OMAE2003-37490.
Peregrine, D., 1983. Water waves, nonlinear Schrödinger equations and their solutions. J. Austral Math. Soc. Ser. B 25 (1), 16–43.
Perić, R., Hoffmann, N., Chabchoub, A., 2015. Initial wave breaking dynamics of Peregrine-type rogue waves: a numerical and experimental study. Eur. J. Mech. - B/Fluids 49 (Part A), 71–76. http://dx.doi.org/10.1016/j.euromechflu.2014.07.002.
Rajendran, S., Fonseca, N., and Guedes Soares, C., 2011. Time domain comparison with experiments for ship motions and strural loads on a container vessel in abnormal waves. In: OMAE 2011–Proceedings of the 30th InternationalConference on Offshore Mechanics and Arctic Engineering. Rotterdam, The Netherlands.
Rajendran, S., Fonseca, N., and Guedes Soares, C., 2013. Estimation of short-term propability distributions of wave induced loads acting on a cruise vessel in extreme seas. In: OMAE 2013–Proceedings of the 32nd InternationalConference on Ocean, Offshore and Arctic Engineering. Nantes, France
Rajendran, S., Fonseca, N., and Guedes Soares, C., 2014. Analysis of vertical bending moment on an ultra large containership induced by extreme head seas. In: OMAE2014–Proceedings of the 33rd InternationalConference on Ocean, Offshore and Arctic Engineering. San Francisco, California, USA
Rajendran, S., Fonseca, N., Guedes Soares, C., 2015a. Simplified Body Nonlinear Time Domain Calculation of Vertical Ship motions and Wave loads in Large Amplitude Waves. Ocean Eng. 107, 157–177.
Rajendran, S., Fonseca, N., Guedes Soares, C., 2015b. Effect of surge motion on the vertical response of ships in waves. Ocean Engg 96, 125–138.
Schmittner, C. and Hennig, J., 2012. Optimization of short-crested deterministic wave sequences voa a phase-amplitude iteration scheme. in: OMAE 2012–Proceedings of the 31st InternationalConference on Ocean, Offshore and Arctic Engineering. Rio de Janeiro, Brazil.
Schmittner, C.E., 2005. Rogue Wave Impact on Marine Structures. Technische Universität Berlin.
Schulz, M., 2001. Ich spürte den Atem Gottes. Der Spiegel, No. 51/2001.
Shemer, L., Alperovich, L., 2013. Peregrine breather revisited. Phys. Fluids 25 (2013), 051701, [doi: 0.1063/1.4807055].
Slunyaev, A., Pelinovsky, E., Sergeeva, A., Chabchoub, A., Hoffmann, N., Onorato, M., Akhmediev, N., 2013. Super-rogue waves in simulations based on weakly nonlinear and fully nonlinear hydrodynamic equations. Phys. Rev. E 88, 012909.
Stansberg, C.T. and Karlsen,S., 2001. Green Sea and Water Impact on FPSO in Steep Random Waves. Rogue Waves 2001 Conference Proceedings.
Suyuthi, A. and Haver,S.K., 2009. Extreme loads due to wave breaking against platform columns. In: Proceedings of the 19th International Offshore and Polar Engineering Conference ISOPE. Osaka, Japan
Torhaug, R., Winterstein, S.R., Braathen, A., 1998. Nonlinear ship loads: stochastic models for extreme response. J. Ship Res. 42 (1), 46–55.
Tromans, P.S., Anaturk, A.R., and Hagemeijer, P., 1991. A new model for the kinematics of large ocean waves - application as a design wave. In: Proceedings of the First International Offshore and Polar Engineering Conference (ISOPE). Edinburgh, United Kingdom.
Watanabe, I., Keno, M., Sawada, H., 1989. Effect of bow flare on shape to wave loads of a container ship. J. Soc. Nav. Arch. Jpn. 166, 259–266.
Zhang, H.D., Guedes Soares, C., Onorato, M., 2015. Modelling of the spatial evolution of extreme laboratory wave crest and trough heights with the NLS-type equations. Appl. Ocean Res. 52, 140–150.
Zhang, H.D., Cherneva, Z., Guedes Soares, C., Onorato, M., 2014. Modeling extreme wave heights from laboratory experiments with the nonlinear Schrödinger Equation. Nat. Hazards Earth Syst. Sci. 14, 959–968.